ELSEVIER

Chemical Geology 186 (2002) 333–344

CHEMICAL GEOLOGY
INCLUDING
ISOTOPE GEOSCIENCE

www.elsevier.com/locate/chemgeo

Solving the production–diffusion equation for finite diffusion domains of various shapes Part I. Implications for low-temperature (U–Th)/He thermochronology

A.G.C.A. Meesters, T.J. Dunai*

Faculty of Earth and Life Sciences, Vrije Universiteit, De Boelelaan 1085, 1081 HV Amsterdam, The Netherlands

Received 30 May 2001; accepted 6 December 2001

Abstract

We propose an accurate, fast and easy-to-use method to derive numerical solutions for production–diffusion equations for finite diffusion domains of various shapes and arbitrary cooling histories. Previous studies provide solutions for spheres, *infinite* cylinders and *infinite* sheets. We extend this range and provide solutions for *finite* bodies, i.e. finite cylinders and rectangular blocks of any aspect ratio. This approach is important as recently, it has become clear that, for example, the physical grain is the diffusion domain for He diffusion in apatite and titanite [J. Geophys. Res. 105 (2000) 2903; Geochim. Cosmochim. Acta 63 (1999) 3845]. We discuss the use of the new approach for forward modelling (U–Th)/He production–diffusion in apatite. Taking results with finite cylinders as a good approximation for apatite crystals, it is found that approximating instead with spheres or infinite cylinders having the same radius yields differences in calculated ages that can easily be as large as 20–35%. The relative differences are most pronounced in thermal histories that spend significant time at or near the closure temperature. On the other hand, reasonable agreement is found with spheres having the same surface to volume ratio.

Keywords: Low-temperature thermochronology; Diffusion; Forward modelling; (U–Th)/He dating

1. Introduction

Since the initial studies of Farley et al. (1996), Lippolt et al. (1994), Wolf et al. (1996), and Zeitler et al. (1987), (U–Th)/He thermochronology utilising apatite quickly developed into a versatile tool for low-temperature geochronology (House et al., 1997, 1998; Reiners et al., 2000; Spotila et al., 1998). To fully exploit the potential of this technique, the accurate knowledge of the diffusion parameters is important (Wolf et al., 1998). Modelling temperature histories of a given area from elevation and/or depth profiles (House et al., 1999; Wolf et al., 1998) requires a suitable description of the geometry of the diffusion domain. To date, invariably spherical diffusion geometries were assumed for modelling He diffusion in apatite (House et al., 1999; Wolf et al., 1996, 1998). This is, however, a simplifying assumption as the physical boundaries of apatite crystals probably denote the size and shape of the diffusion domain

* Corresponding author. Fax: +31-6462457.
E-mail address: dunt@geo.vu.nl (T.J. Dunai).

0009-2541/02/$ - see front matter
PII: S0009-2541(01)00422-3

(Farley, 2000), which in turn is clearly not spherical. A finite cylinder is a much closer approximation of apatite than a sphere, or an infinite cylinder as proposed by Farley (2000) (typical length/radius for granitic apatites is, e.g. $\sim 4-8$). To date, however, there is no feasible procedure, which allows the accurate numerical solution for the production–diffusion equation for finite cylinders. In this paper, we provide an efficient method that can be used not only for spherical and infinite geometries, but also for *finite cylinders* and *rectangular blocks of any shape*. The latter may be of use for other minerals such as titanite, for which it is demonstrated that the diffusion domain is the physical grain size (Reiners and Farley, 1999). As this method can be applied to spherical and infinite geometries, we use this to check the consistency of our modelling results with previously published exact solutions for special cooling histories (Carslaw and Jaeger, 1959; Dodson, 1973; McDougall and Harrison, 1999). In this paper, we demonstrate that most arbitrary shapes can be approximated by a sphere under the condition that this sphere has the same surface to volume ratio.

For the time being, effects of a zoned distribution of parent nuclides, and of α-ejection, are neglected. In a second paper (Meesters and Dunai, 2002) (henceforth called part II), the method will be extended to incorporate these effects. The methods and results presented in part I can also be applied to Ar geochronology.

2. Methods

2.1. Description of the problem, and solutions in the literature

The problem that we are facing can be stated in mathematical terms as follows. There is a diffusion domain of a given shape and size. In it, radioactive decay produces a daughter isotope of unknown concentration $C(x,y,z,t)$ (mol per volume unit). The daughter isotope is produced at a rate U (source, mol per volume unit per time unit). It is understood that U is either a constant or an exponentially decaying function of time. In this paper (except for Appendix A), we restrict ourselves to a place-independent U: $U = U_R(t)$. In part II, the case of a place-dependent U will receive an elaborate treatment. The daughter is subject to diffusion, and the diffusion coefficient D is a given function of time (but decidedly not of place). A further assumption is that the transport of the daughter into the environment is such that the concentration is always zero at the boundary. We are concerned with processes starting at an initial time t_{init}, and ending at the present time t_{pres}. Our problem is now to compute the spatially averaged value of C, C_{av}, at the final stage. Eventually, it may be also interesting to compute the temporal evolution of $C_{av}(t)$. The most interesting entity is the ratio C_{av}/U, which corresponds to the measured age t_c. (unless t_c is not much smaller than the decay time τ ($\tau = 1/\lambda$, λ = decay constant), in which case $C_{av}/U = \tau(e^{t_c/\tau} - 1)$).

To solve the production–diffusion equation, finite difference methods are generally inappropriate. The Crank–Nicolson method (Crank, 1975; Crank and Nicolson, 1947), which belongs to this class, is feasible for domains that can be reduced mathematically to a one-dimensional form. This is the case for infinite plane sheets and also for spheres and infinite cylinders. The method has recently been applied successfully to (U–Th)/He (Wolf et al., 1998), assuming spherical diffusion domains. However, if such a reduction is impossible, finite difference methods become comparatively very slow and practically unfeasible.

A more appropriate method is based on the decomposition of the problem into eigenmodes. The application to constant D (Carslaw and Jaeger, 1959) is well known. Dodson (1973) investigated the case of an exponentially decaying $D(t)$, as often used in geochronology. The application of this method to arbitrary $D(t)$, which is of interest of us, has been discussed by Lovera et al. (1989) and followed by McDougall and Harrison (1999, Chap. 6). The discussion of this point is continued in Section 2.2.

Another important issue is the derivation of the correct values for D as used in the calculations. For each temperature, values for D can be calculated using the Arrhenius equation (see, e.g. McDougall and Harrison, 1999) and experimentally derived values of D_0 and E_a. As there are various approaches to interpret diffusion experiments and because some of these approaches will affect modelling results, they will be discussed here.

In Ar geochronology, it is customary to report D_0/a^2 values (where a is the characteristic dimension of the diffusion domains; Dodson, 1973) (McDougall and Harrison, 1999 and references therein). The consequent application of this approach largely mends the complications related to geometry that are discussed in this paper. Consequent application in this context means that the geometry of the sample on which the diffusion experiment is performed is equivalent to that of the measured (unknown) sample used for modelling constraints, and that throughout the calculations, the same term D_0/a^2 is used (i.e. the same diffusion domain size). Then, effects of shape and dimensions as described below will cancel each other out in the course of the calculations. In Ar geochronology, usually, crushed fragments of much larger crystals are used, both for diffusion experiments and for geochronological studies, such that its possible to design experiments that meet the condition of consequent application. The use of crystal fragments has the additional benefit that the assumption of a rectangular concentration profile, essential for the correct calculation of the diffusion parameters (Fechtig and Kalbitzer, 1966, p. 71; see also below), is usually met on the fragment scale, while this is often not true for the original, unfragmented crystal.

In (U–Th)/He-geochronology, both D_0/a^2 (e.g. Reiners and Farley, 1999; Wolf et al., 1996; Zeitler et al., 1987) and D_0 values have been reported (Farley, 2000; Reiners and Farley, 1999). The use of D_0 seems justified at least for apatite and titanite where the grain size is probably the diffusion domain size (Farley, 2000; Reiners and Farley, 1999, 2001). This is important as the successful approach as used in Ar geochronology, i.e. consequently using D_0/a^2, cannot be straightforwardly applied to (U–Th)/He-geochronology. This has to do with (i) the usually small size of the most commonly used minerals (apatite, titanite, zircon), (ii) the relative ease of He-loss and (iii) the significant emission distance of α-particles in minerals (Farley et al., 1996). If, for example, apatites of geological samples are used for diffusion experiments, e.g. to characterize an apatite population for a given thermochronological study (Reiners and Farley, 2001), α-ejection and He-loss during the cooling of the natural sample will result in rounded concentration profiles. While the rounding due to ejection can be accurately described in some cases (homogenous U and Th concentration) (Farley et al., 1996), the rounding due to diffusive loss of He is a priori an unknown, as the cooling history is not yet known but is the goal of the thermochronological study. Fechtig and Kalbitzer (1966), whose equations are invariably used to interpret stepwise heating experiments (e.g. (Farley, 2000; Reiners and Farley, 1999, 2001; Wolf et al., 1996)), are explicit about the consequences of unconstrained concentration profiles: "The disturbance of the square profile can only be neglected when the fraction released by the experiment is several times higher than the original loss; in this case, the resulting diffusion coefficient will be right. In particular, if a sample with argon losses [in our case helium losses] is taken for diffusion experiments, one should be aware of the violation of the boundary conditions. The apparent diffusion constants will come out too low, and the activation energies too high" (Fechtig and Kalbitzer, 1966, p. 71). The way around the problem that is pointed out by Fechtig and Kalbitzer (1966), release of large fractions of gas in the experiments, is problematic (Dunai, 2000) and in the case of apatite virtually impossible to achieve, if the apparent change of diffusion mechanism at temperatures >265 °C (Farley, 2000) is real. Suitable experiments at temperatures <265 °C would last weeks to several months, if not years, and thus are impractical. It is likely that the diffusion coefficients obtained by Reiners and Farley (2001) and Wolf et al. (1996) on samples with rounded concentration profiles are hereby inaccurate and that, e.g. differences in calculated T_C of geological samples and Durango apatite as described by Reiners and Farley (2001, p. 417) are at least in part experimental artifacts due to violation of the boundary conditions described by Fechtig and Kalbitzer (1966).

The remaining option is to use fragments of large crystals (Dunai, 2000; Farley, 2000; Reiners and Farley, 1999; Wolf et al., 1996), largely eliminating the problem of rounded concentration profiles. However, if fragments are used, the D_0/a^2 from those experiments cannot be used analogous to Ar geochronology for natural crystals as the geometry of shards and the crystals is clearly different and the characteristic dimension a will be different in most cases. Therefore, D_0 has to be used with an appropriate value for a (Reiners and Farley,

2001) in accordance with the geometry of the crystals.

The D_0 and E_a as can be obtained from fragments (e.g. Farley, 2000) are material properties that can be applied to all geometries if the diffusion is isotropic. For the remainder of this paper, we will assume isotropic diffusion, which at least for apatite seems to be justified within the experimental uncertainties (Farley, 2000). Anisotropic diffusion could be incorporated in the calculations presented here; however, in the light of presently available experimental data, we believe that this is not yet mandated. Another assumption that underlies our calculations is that the grain is the diffusion domain size (Farley, 2000; Reiners and Farley, 1999, 2001), i.e. that the modelled grains are free of cracks and other fast tracks for diffusion. For the calculations, we use D_0 and E_a of Wolf et al. (1996) as these values have been used in Wolf et al. (1998), to which we will compare our calculations (D_0 is obtained using $a = 60$ μm). For actual calculations that go beyond the qualitative discussion presented here, the more recent values of Farley (2000) should be used as a model for He diffusion in apatite. The actual differences between using the values of Wolf et al. (1996) and Farley (2000) are, however, small compared to the effects discussed in this paper. In the future, studies that describe, e.g. the potential influence of composition on He diffusion will further increase the accuracy of the modelling results.

2.2. Our method

In this paper, we describe an easy-to-use version of the eigenmode-method. The method is equivalent to the one of Lovera et al. (1989), but is simpler in several respects. Moreover, it is extended to other shapes to facilitate the application to domains that have the shape of crystals. Specifically, besides the sphere, infinite cylinder and plate already discussed by Lovera et al. (1989), also the rectangular block and the finite cylinder are treated here. This, however, necessitates a different notation (mainly since there is no longer a unique length scale).

It is shown in Appendix A that the spatial average $C_{av}(t)$ can be expressed as

$$C_{av}(t) = \sum_{n=1}^{\infty} c_n(t) \tag{1}$$

in which $c_n(t)$ is the contribution of the n-th eigenmode. Sometimes (see Section 2.3), the eigenmodes are naturally labeled with more than one index, so that more than one summation sign is required. In the following, a single index is used for convenience.

The c_n evolve according to (see Appendix A, Eq. (26))

$$\frac{dc_n}{dt} = -\mu_n D(t) c_n(t) + \gamma_n U_R(t) \tag{2}$$

in which μ_n and γ_n are parameters depending on geometry. Consequently, evaluating $C_{av}(t)$ entails three steps. First, the coefficients μ_n and γ_n should be determined. Second, the differential equation for $c_n(t)$ should be solved numerically. Third, the results of $c_n(t)$ should be summed to obtain $C_{av}(t)$. The latter step is nontrivial as there are in principle infinitively many of them. We now consider the three necessary steps in sequence. The parameters μ_n and γ_n are given in the section on geometry (Section 2.3) for "ideal" shapes, assuming a place-independent U. We note that if the source is place-dependent, as is the case when α-ejection is properly accounted for, the γ_n values should be adjusted, whereas the μ_n values remain unchanged (see part II). Our method to solve Eq. (2) is presented below. Its derivation is given in Appendix A. A comparison with Lovera et al. (1989) is given in Appendix B. It will be seen that although the methods may look very different at first sight, the results are equivalent. Our method, however, has a simpler derivation, and appears easier to use.

The resulting procedure to evaluate $c_n(t)$ is as follows. Let the diffusion coefficient be given as an array of values: $D_1, D_2, \ldots, D_N$, corresponding to the times $t_1, t_2, \ldots, t_N$, in which $t_N = t_{pres}$. The times, not necessarily equidistant, should of course be chosen so that they yield a reasonable resolution of $D(t)$. The source function U_R should be given as either a constant $U_{R,0}$, or it should have the form $U_{R,0} \cdot \exp(-t/\tau)$. The array F is defined as:

$$F_j = t_j \text{ or } F_j = \tau(1 - \exp(-t_j/\tau)) \tag{3}$$

for constant or decaying source-strength, respectively.

From the input arrays, intermediate arrays ξ and F' are derived. The first represents the time integral of D:

$$\xi(t) = \int_{t1}^{t} D(\theta) d\theta \tag{4}$$

Discrete values are computed by $\xi_1 = 0$ and subsequently

$$\xi_{j+1} = \xi_j + \frac{D_j + D_{j+1}}{2}(t_{j+1} - t_j) \tag{5}$$

for $j = 1, 2, \ldots, N-1$. The array F' represents $\mathrm{d}F/\mathrm{d}\xi$ and is constructed as

$$F'_j = \frac{F_{j+1} - F_j}{\xi_{j+1} - \xi_j} \tag{6}$$

for $j = 1, \ldots, N-1$.

Now, the expression for $c_n(t_{\mathrm{pres}}) = c_n(t_N)$ is (see also Appendix A, Eqs. (32), (38), (40))

$$c_n(t_N) = x + U_{\mathrm{R},0}\frac{\gamma_n}{\mu_n}\sum_{j=1}^{N-1}(\beta_{N,j+1} - \beta_{N,j})F'_j \tag{7}$$

in which

$$\beta_{N,k} = \exp(-\mu_n(\xi_N - \xi_k)) \tag{8}$$

If the concentration is initially zero, $x = 0$, otherwise

$$x = c_n(t_1)\exp(-\mu_n\xi_N) \tag{9}$$

To facilitate computations with Eq. (7), it can be used that β decreases with decreasing second index, and is effectively zero for sufficiently low indices (corresponding to times of fast diffusion, or times preceding fast diffusion). $C_{\mathrm{av}}(t_N)$ is found by summing $c_n(t_N)$ over all eigenmodes (all n; Eq. (1)). Finally, $C_{\mathrm{av}}(t_N)/U_{\mathrm{R}}(t_N)$ is the quantity that should be compared to the measured ages. On working out, $U_{\mathrm{R},0}$ does not occur in the expression if x is zero. Final values $c_n(t_N)$ can be calculated using Eq. (7) without first calculating earlier values of c_n. If desired, one can of course compute the whole time series. To find $C_{\mathrm{av}}(t_J)$ for some arbitrary t_J in the set $t_1, \ldots, t_N$, one should replace N with J in Eqs. (7)–(9).

Finally, the summation problem has to be considered. In practice, instead of the infinite sum in Eq. (1), one can only compute partial sums. By the M-th partial sum $\sum_M$, we understand

$$\sum\nolimits_M = \sum_{j=1}^{M} c_j(t) \tag{10}$$

if there is one index,

$$\sum\nolimits_M = \sum_{j=1}^{M}\sum_{k=1}^{M} c_{j,k}(t) \tag{11}$$

if there are two indices, etc. For modest values of M, the difference between $\sum_M$ and $\sum_\infty$ can be considerable. Fortunately, this can be remedied since $\sum_M$ appears experimentally to have a regular dependence on M as M becomes large: specifically, one obtains a fairly straight line by plotting $\sum_M$ as a function of $y_M = 1/(M + 1/2)$, as illustrated in Fig. 1. We used this by taking the best-fitting straight line (in least-squares sense) through the points $M = 11$ to $M = 15$, and then calculated the value of this line for $y_M = 0$ (or $M = \infty$), thus obtaining an accurate estimate for $\sum_\infty$.

The attractiveness of this method decreases rapidly if the number of indices increases. With one index (as for the sphere), one needs the first 15 c_n values, but with two or three indices, 15^2 or 15^3 values are required to obtain the same accuracy; note that $15^3 = 3375$. Fig. 1 suggests that good estimates can be obtained already from lower order c_n. This is indeed the case for the space-independent sources of this paper. However, with space-dependent sources as will be considered in part II, it appears practically impossible to use less than 15 levels, as will be seen.

The results of this method have been compared to exact results, which are known for cases with constant D (Carslaw and Jaeger, 1959) and for cases with $D(t)$ decaying as an exponential function of t (Dodson, 1973; McDougall and Harrison, 1999). Irrespective of the domain size, an excellent agreement was found.

2.3. Geometry

The required information about geometry consists of the eigenvalue μ_n and a dimensionless number γ_n for each n-th eigenmode. The method to compute these is indicated in Appendix A. As in this paper, we only consider a source function of the form $U_{\mathrm{R}}(t)$, $S_{\mathrm{place}} = 1$ in Appendix A. For this case, the values of μ_n and γ_n are related to a classical problem, namely the cooling of a body (with constant D and no heat source) from an initial constant temperature T_0, with

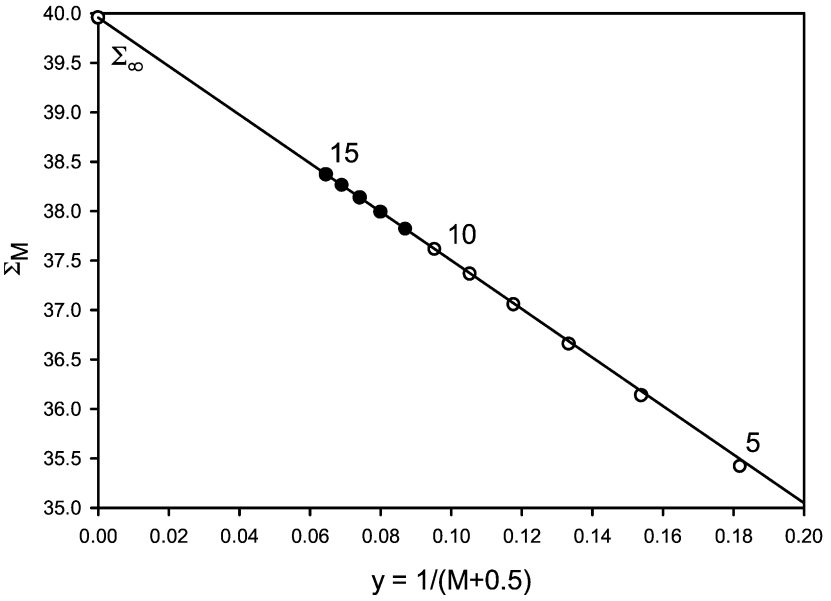

Fig. 1. Illustration of determining an infinite sum $\sum_\infty$ from partial sums $\sum_{11}\ldots\sum_{15}$. Discussion is given in the text.

$T=0$ at the boundary. The corresponding expression for the average temperature is known to be

$$T_{\mathrm{av}}(t) = T_0 \sum_{n=1}^{\infty} \gamma_n \exp(-\mu_n D t) \tag{12}$$

Carslaw and Jaeger (1959) elaborately discuss this problem for many shapes, and from the expressions given there, μ_n and γ_n can be easily inferred. Eigenmodes with spatial average zero are skipped.

For a *sphere* of radius a,

$$\mu_n = \left(\frac{n\pi}{a}\right)^2; \quad \gamma_n = \frac{6}{(n\pi)^2} \tag{13}$$

for $n=1, 2, 3, \ldots$

For a rectangular block of edge-lengths a, b, c, each eigenmode is labeled with three indices, ℓ, m, and n, each of which runs from 1 to infinity, and

$$\mu_{\ell,m,n} = \pi^2 \left(\frac{(2\ell-1)^2}{a^2} + \frac{(2m-1)^2}{b^2} + \frac{(2n-1)^2}{c^2} \right) \tag{14}$$

$$\gamma_{\ell,m,n} = \frac{512}{\pi^6} \frac{1}{(2\ell-1)^2} \frac{1}{(2m-1)^2} \frac{1}{(2n-1)^2}. \tag{15}$$

If one of the edge lengths of the block, say c, is infinite, the index n disappears, the corresponding term in the expression for μ is dropped, and

$$\gamma_{\ell,m,n} = \frac{64}{\pi^4} \frac{1}{(2\ell-1)^2} \frac{1}{(2m-1)^2} \tag{16}$$

If b is also infinite, we have an infinite plate. The indices m and n disappear, the corresponding terms in the expression for μ are dropped, and

$$\gamma_{\ell} = \frac{8}{\pi^2} \frac{1}{(2\ell-1)^2} \tag{17}$$

For the cylinder, the computations are somewhat more involved. One needs the zeros of the Bessel function J_0: $j_{0,1}=2.40482\ldots$; $j_{0,2}=5.52007\ldots$; etc. These values are listed in Table 9.5 of Abramowitz and Stegun (1965).

For a cylinder of radius a and height h, the eigenmodes are labeled with two indices, m and n, each running from 1 to infinity, and

$$\mu_{m,n} = \left(\frac{j_{0,m}}{a}\right)^2 + \left(\frac{(2n-1)\pi}{h}\right)^2;$$
$$\gamma_{m,n} = \frac{32}{(j_{0,m}(2n-1)\pi)^2} \tag{18}$$

If h is infinite, there is only one index and

$$\mu_m = \left(\frac{j_{0,m}}{a}\right)^2; \quad \gamma_m = \frac{4}{j_{0,m}^2} \tag{19}$$

3. Discussion

After providing a method to derive numerical solutions for the production–diffusion equation for finite and infinite diffusion domains of various shapes, we now discuss the implications for low-temperature geochronology. As an example, we will focus on (U–Th)/He thermochronology. A great potential of the (U–Th)/He method is that, depending on the cooling history of a rock, significant information can be obtained about the timing and duration of the samples passage through the partial retention zone (PRZ; Wolf et al., 1998). The PRZ for He in apatite extends from ~40 to ~85 °C (Wolf et al., 1998). There is little difference between the PRZ and typical environmental temperatures; thus, geological interpretations of (U–Th)/He data are potentially very sensitive to deviation in assumptions used to model the results. One of those assumption is the shape of the diffusion domain, which we investigate here.

Wolf et al. (1998) conducted a thorough investigation of the temperature sensitivity of (U–Th)/He thermochronology utilizing apatite. In the study of Wolf et al. (1998), explicitly a spherical diffusion domain is assumed that is smaller than the physical grain. Recently, however, Farley (2000) demonstrated that the physical grain is the diffusion domain and suggested that the infinite cylinder is the most appropriate geometry for modeling He-diffusion. In the following, we use some of the thermal histories discussed by Wolf et al. (1998) to illustrate the sensitivity of diffusion to domain shape. We will show that both the assumption of a sphere (Wolf et al., 1998) and the assumption of an infinite cylinder (Farley, 2000), can lead to significant deviations if the diffusion domain is indeed the physical grain, i.e. rather of finite cylindrical shape.

In Fig. 2, He age evolution curves are plotted for several representative time–temperature paths. Please note that the format of this figure and input parameters for the thermal histories are the same as used by Wolf et al. (1998) in his Fig. 5. For geological significance of those cooling histories, we refer the reader to Section 3.1. in Wolf et al. (1998). For the calculation, we used time steps of 5 Ma and a time-independent source strength; for history 5, the time steps were reduced to 1 Ma for the last 5 Ma. For histories with a step in the temperature (histories 1 and 3), an adjusted version of Eq. (5) has been used

$$\xi_{j+1} = \xi_j + D_j(t_{j+1} - t_j) \tag{20}$$

to account for the fact that the temperature remains constant over each time step, rather than being continuous and piecewise linear as is otherwise assumed.

We calculated He evolution curves for spheres (radius 60 μm), cubes (height 120 μm), rectangular blocks (height $h_1 = 120$ μm, $h_2 = h_3 = 240$ μm), finite cylinders (radius 60 μm, length 240 μm) and infinite cylinders ($r = 60$ μm), utilizing our equations derived above. Note that the minimum dimension is the same in all cases (120 μm). In all examples shown in Fig. 2, we obtain the same results for spheres as Wolf et al. (1998). We take this as an indication of the reliability of our method to reproduce results obtained by the Crank–Nicolson method (Crank and Nicolson, 1947; Wolf et al., 1998).

It is evident from Fig. 2 that for fast and monotonic cooling (histories 1 and 2), the differences between the He age evolution curves is relatively small (but still up to 10% in final ages for history 2). For temperature histories where the apatites spend significant time in the PRZ (histories 3, 4, and 5, Fig. 2) the differences between the various geometries, however, can increase to up to 40% (e.g. difference between the rectangular block and sphere relative to age obtained for the sphere, history 5). While the maximum difference is not necessarily significant for apatites, it clearly serves to illustrate that the shape of diffusion domains is not irrelevant for the outcome of models predicting He accumulation in minerals. Comparing the results for spheres to geometries more relevant to He diffusion in apatite, i.e. finite and infinite cylinders, the relative differences are still large, up to 20% and 35%, respectively. We therefore conclude that it is important to properly consider diffusion domain shapes, at least in low-temperature geochronology. We propose for the time being that finite cylinders be used to model apatite. We recommend that the radius used is derived according to $r = (d_{\max} + d_{\min})/4$,

where d_{max} and d_{min} are the outer and inner diameter of the hexagonal prism, respectively. The length of the apatites should be the prism length, plus the 1/4th of the height of the terminating pyramids, if they are present (the latter term will usually be negligible).

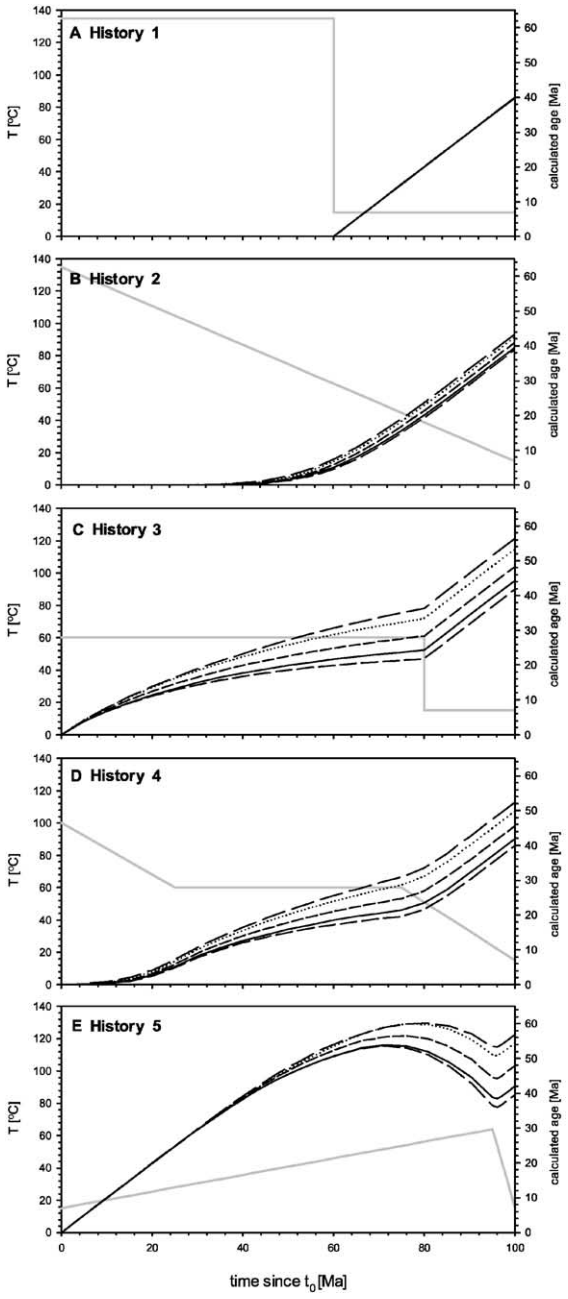

The bodies modeled in Fig. 2 have different surface to volume ratios (S/V) and we will show in the following that these differences are significant for modeling accumulation of He in these and other bodies. The S/V ratios of the bodies in Fig. 2 are: cube and sphere both 0.05 μm^{-1}, finite cylinder 0.0417 μm^{-1} and infinite cylinder and rectangular block both 0.0333 μm^{-1}. As can be seen from histories 3–5 in Fig. 2, bodies with the same S/V ratio are more similar to each other in their accumulation behavior than to those with different S/V ratio (see also Lagerwall and Zimen, 1964). For example, the infinite cylinder is more comparable to the rectangular block than to the finite cylinder, and is most distinct from the sphere. The intermediate position of the finite cylinder seems to be in agreement with its intermediate S/V ratio. To better illustrate the effect of the S/V ratio, we also present in Fig. 3 the same thermal histories as in Fig. 2, but calculated for bodies that have the same S/V ratio as a sphere with 60 μm radius, i.e. 0.05 μm^{-1}. The bodies modeled in Fig. 2 have the same aspect ratio as those in Fig. 1, i.e. have the same shape (cube same as Fig. 2; block $h_1 = 80$ μm, $h_2 = h_3 = 160$ μm; finite cylinder $r = 50$ μm, $l = 200$ μm; infinite cylinder $r = 40$ μm). It is evident from Fig. 3 that that the differences between the various bodies are greatly reduced, the biggest "outlier" is the infinite cylinder with a maximum deviation of ~7% relative to the sphere. For practical purposes, however, considering the analytical uncertainties and uncertainties involved with α-ejection correction (Farley et al., 1996), the histories of most bodies are equally valid (at least for bodies with modest aspect ratios). Therefore, we conclude that finite cylinders with an aspect ratio typical for apatites can be modeled as spheres of the same S/V ratio (these

Fig. 2. Apatite He age evolution curves of various grain geometries (black lines) for several representative time–temperature paths (solid grey line). The format and thermal parameters to model for time–temperatures are the same as used for Fig. 5 in Wolf et al. (1998). In plots A–E, the sequence of the evolution curves is the same. The lowest ages are always obtained for spheres. In increasing order, the spheres are followed by the cube, finite cylinder, infinite cylinder and rectangular block (medium dashed line = sphere; solid line = cube; short dashed line = finite cylinder; dotted line = infinite cylinder; long dashed line = rectangular block). Dimensions of the modeled bodies are given in the text as is a more extensive discussion.

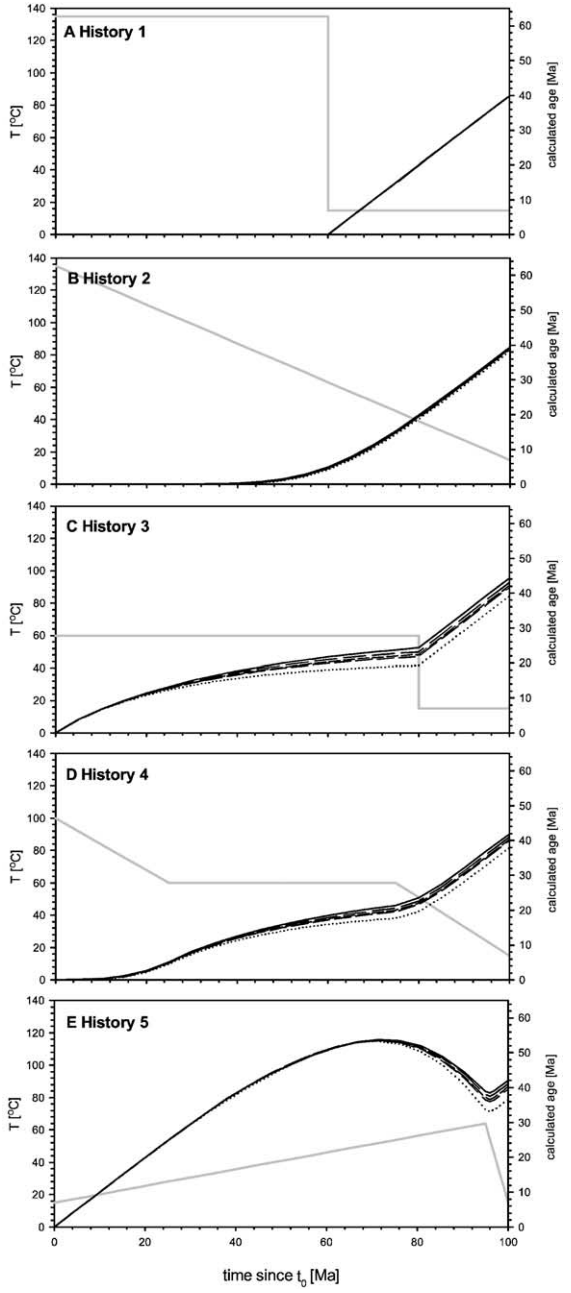

Fig. 3. As Fig. 2 but calculated for grains with the same surface to volume ratio as a sphere of 60 μm radius. The shapes (i.e. aspect ratios) of the grains are the same as in Fig. 2. The linestyles are the same as in Fig. 2. Please note that the age sequence for the different bodies is not the same as in Fig. 2 (medium dashed line = sphere; solid line = cube; short dashed line = finite cylinder; dotted line = infinite cylinder; long dashed line = rectangular block). Further discussion is given in the text.

"model spheres" will always have a radius greater than the radius of the physical apatite grains, 20% greater in above case). This approach may be advantageous for inverse modeling when a 10-fold decrease of computation time is desirable. The approximation of a body of interest by spheres of same S/V ratio can probably also be used for shapes not covered by our method presented above.

4. Conclusions

(1) The method we derived for solving production–diffusion equations can be used for various crystal shapes for which no solutions existed yet, e.g. finite cylinders and rectangular blocks.

(2) The shape of diffusion domains is important for modeling He accumulation in apatite grains during cooling histories that spend significant time in the partial retention zone. Using spheres or infinite cylinders instead of finite cylinders with the same radius yields differences in calculated ages of up to 35%.

(3) The surface to volume ratio of mineral grains of different shapes and aspect ratios is an important parameter describing the influence of geometry on diffusion behavior.

(4) The diffusion behavior of mineral grains with modest aspect ratio can be approximated by spheres of identical surface to volume ratio.

The implications of zoned U and Th distribution and of α-ejection will be discussed in part II.

Acknowledgements

We are grateful to Marlies ter Voorde for useful suggestions in making this paper more readable. The constructive reviews of Peter Zeitler and Ken Farley improved the manuscript considerably. This is NSG-publication no. 20011003. **[RR]**

Appendix A. Solution of the production–diffusion equation

In the following, the He source-function is allowed to depend on both place and time, so the it can be written as $S_{\text{place}}(x,y,z)U_{\text{R}}(t)$ in which S_{place} is dimen-

sionless. In the present paper, $S_{\text{place}} = 1$, but in part II (Meesters and Dunai, 2002), the more general case will be considered. The production–diffusion equation to be solved is

$$\frac{\partial C}{\partial t} = D(t)\,\nabla^2 C + S_{\text{place}}(x,y,z)U_{\text{R}}(t) \tag{21}$$

with C an unknown function of place and time, and $D(t)$, $U_{\text{R}}(t)$ and $S_{\text{place}}(x,y,z)$ known functions. The equation holds for a diffusion domain of a certain size and shape, and C is zero at the boundary.

For any domain shape, there are infinitely many eigenfunctions $u_n(x,y,z)$ (zero at the boundary) and corresponding eigenvalues μ_n satisfying the equation

$$\nabla^2 u_n = -\mu_n u_n. \tag{22}$$

Moreover, every function arising in diffusion problems can be expressed in eigenfunctions:

$$C(x,y,z,t) = \sum_{n=1}^{\infty} f_n(t)u_n(x,y,z), \tag{23}$$

with $f_n(t)$ as yet unknown. We also need the expression

$$S_{\text{place}}(x,y,z) = \sum_{n=1}^{\infty} s_n u_n(x,y,z), \tag{24}$$

to express $S_{\text{place}}(t)$ in eigenfunctions; the s_n are assumed to be known. Substitution of these two expressions in the production–diffusion equation (Eq. (21)) and working out using Eq. (22) yields an equation for each eigenmode separately, namely

$$\frac{\mathrm{d}f_n}{\mathrm{d}t}(t) = -\mu_n D(t) f_n(t) + s_n U_R(t). \tag{25}$$

Since we are only interested in the spatial average, we multiply this with the spatial average of u_n: $u_{n,\text{av}}$, to obtain

$$\frac{\mathrm{d}c_n}{\mathrm{d}t} = -\mu_n D(t) c_n(t) + \gamma_n U_{\text{R}}(t), \tag{26}$$

in which

$$c_n(t) = f_n(t)u_{n,\text{av}}, \tag{27}$$

is the contribution of the n-th eigenmode to the average concentration, and

$$\gamma_n = s_n u_{n,\text{av}}. \tag{28}$$

It follows that the required geometrical information is entirely contained in μ_n and γ_n.

The solution to Eq. (26) is

$$c_n(t) = c_n(t_{\text{init}})\exp(-\mu_n \xi(t)) + \gamma_n H_n(t), \tag{29}$$

in which

$$\xi(t) = \int_{t_{\text{init}}}^{t} D(\theta)\mathrm{d}\theta, \tag{30}$$

and

$$H_n(t) = \int_{t_{\text{init}}}^{t} \mathrm{d}\theta U_R(\theta)\exp\big(-\mu_n(\xi(t) - \xi(\theta))\big) \tag{31}$$

The solution to Eq. (25) has the same form (with s_n instead of γ_n), but we do not need it as we are only interested in spatial averages.

For the present purpose, we assume that C is initially zero, hence $f_n(t_{\text{init}})$ and $c_n(t_{\text{init}})$ are zero too. It then follows that

$$C_{\text{av}}(t_N) = \sum_{n=1}^{\infty} c_n(t_N) = \sum_{n=1}^{\infty} \gamma_n H_n(t_N). \tag{32}$$

$H_n(t)$ remains to be determined. To deal with the difficult exponent in Eq. (31), it is better to choose as a new integration variable $\chi = \xi(\theta)$ rather than θ itself, yielding

$$H_n(t) = \int_0^{\xi} \mathrm{d}\chi \frac{U_{\text{R}}(\chi)}{D(\chi)}\exp(-\mu_n(\xi - \chi)), \tag{33}$$

in which $\xi = \xi(t)$, and by "$U_{\text{R}}(\chi)$" we understand $U_{\text{R}}(\theta)$ expressed as a function of the "transformed time" $\chi = \xi(\theta)$.This expression is, however, not very attractive for numerical use, as the denominator D is a very variable function, and sometimes effectively zero.

To deal with this, we write U_{R}/D as a derivative and by assuming that $U_{\text{R}}(t)$ is either a constant $U_{\text{R},0}$ or $U_{\text{R}}(t) = U_{\text{R},0}\ \exp(-t/\tau)$, we can define a function F using

$$F(t) = t \quad (\tau = \infty) \text{ or}$$
$$F(t) = \tau(1 - \exp(-t/\tau)) \quad (\tau < \infty).$$

It follows that

$$\frac{U_{\mathrm{R}}}{D}=\frac{U_{R,0}}{D}\frac{\mathrm{d}F}{\mathrm{d}t}=\frac{U_{\mathrm{R},0}}{D}\frac{\mathrm{d}\chi}{\mathrm{d}t}\frac{\mathrm{d}F}{\mathrm{d}\chi}=U_{\mathrm{R},0}\frac{\mathrm{d}F}{\mathrm{d}\chi}, \qquad (35)$$

since $\mathrm{d}\chi/\mathrm{d}t=D$ because of the definition of $\chi=\xi(t)$. Hence, the integral can be rewritten as

$$H_n(t)=U_{\mathrm{R},0}\int_0^{\xi}\mathrm{d}\chi\frac{\mathrm{d}F}{\mathrm{d}\chi}(\chi)\exp(-\mu_n(\xi-\chi)). \qquad (36)$$

In practice, a number of times t_1 ($=t_{\mathrm{init}}$), t_2, …, t_N ($=t_{\mathrm{pres}}$) is given, with corresponding diffusion coefficients D_1, D_2, …, D_N as well as the values F_1, F_2, …, F_N. The corresponding ξ_j can be estimated by

$$\xi_1=0;\quad \xi_{j+1}=\xi_j+(D_j+D_{j+1})(t_{j+1}-t_j)/2. \qquad (37)$$

The integral $H_n(t_N)$ can then be written as a sum over intervals:

$$H_n(t)=U_{\mathrm{R},0}\sum_{j=1}^{N-1}\int_{\xi_j}^{\xi_{j+1}}\mathrm{d}\chi\frac{\mathrm{d}F}{\mathrm{d}\chi}(\chi)\times\exp(-\mu_n(\xi_N-\chi)). \qquad (38)$$

A feasible approximation is

$$\frac{\mathrm{d}F}{\mathrm{d}\chi}(\chi)\approx\frac{F_{j+1}-F_j}{\xi_{j+1}-\xi_j}\qquad(\xi_j\le\chi\le\xi_{j+1}). \qquad (39)$$

The ensuing value for the integrals is

$$\int_{\xi_j}^{\xi_{j+1}}\mathrm{d}\chi\frac{\mathrm{d}F}{\mathrm{d}\chi}(\chi)\exp\big(-\mu_n(\xi_N-\chi)\big)\approx\frac{F_{j+1}-F_j}{\xi_{j+1}-\xi_j}\frac{1}{\mu_n}\big(\exp\big(-\mu_n(\xi_N-\xi_{j+1})\big)-\exp\big(-\mu_n(\xi_N-\xi_j)\big)\big). \qquad (40)$$

By this, the problem is solved.

Appendix B. Comparison with the method of Lovera et al. (1989)

This section is intended for readers acquainted with the method and notation of Lovera et al. (Lovera et al., 1989; McDougall and Harrison, 1999); therefore, we employ the same notation without explanation. It will be shown that their method is equivalent to ours, which is not immediately obvious. It will also be shown how, in accordance with our more straightforward method, some of the expressions of Lovera et al. (1989) can be considerably streamlined.

Lovera et al. (1989) use a function I_n, but a more fundamental quantity appears to be H_n (our notation):

$$H_n(\xi)=I_n(\xi)-\exp(-\lambda\tau\theta_0), \qquad (41)$$

as will be seen. The right-hand side occurs in the expressions for the argon fluxes that they derive, but the fundamental character of this quantity is insufficiently noted. Using their expression for $I_n(t)$, one finds as expression for $H_n(t)$:

$$H_n(\xi)=\exp(-\alpha_n^2\xi)-\exp(-\lambda\tau\theta_0)+\alpha_n^2\int_0^{\xi}\mathrm{d}\chi\exp(-\lambda\tau\theta(\chi))\times\exp\big(-\alpha_n^2(\xi-\chi)\big). \qquad (42)$$

An important point is that it can be shown that this is equivalent to

$$H_n(\xi)=\int_0^{\xi}\mathrm{d}\chi\frac{\mathrm{d}}{\mathrm{d}\chi}(1-\exp(-\lambda\tau\theta(\chi))\times\exp(-\alpha_n^2(\xi-\chi)), \qquad (43)$$

by applying integration by parts to the latter form, and using that $\theta(\xi)=\theta_0$ and $\theta(0)=0$. This new form for H_n corresponds to Eq. (36).

For the evolution of the concentration, Lovera et al. (1989) give the expression

$$C\big(\overrightarrow{x},\theta_0\big)/C_0=1-\exp(-\lambda\tau\theta_0)-\sum_{n=1}^{\infty}(-1)^{n+1}\alpha_n^{-1}U\big(\alpha_n\overrightarrow{x}\big)(1-I_n). \qquad (44)$$

However, this can be considerably simplified by substitution of $I_n=H_n+\exp(-\lambda\tau\theta_0)$, and using the

equation for the expansion of the unity function in eigenfunctions:

$$\sum_{n=1}^{\infty}(-1)^{n+1}\alpha_n^{-1}U\left(\alpha_n\overrightarrow{x}\right)=1, \tag{45}$$

which yields

$$C(\overrightarrow{x},\theta_0)/C_0=\sum_{n=1}^{\infty}(-1)^{n+1}\alpha_n^{-1}U\left(\alpha_n\overrightarrow{x}\right)H_n. \tag{46}$$

This is not only simpler than the old form, but also contains a faster converging sum. Averaging over the spatial domain, using that the average of $U(\alpha_n x)$ is $(-1)^{n+1}b/\alpha_n$, yields

$$C_{\mathrm{av}}(\theta_0)/C_0=b\sum_{n=1}^{\infty}H_n/\alpha_n^2, \tag{47}$$

corresponding to Eq. (32).

References

Abramowitz, M., Stegun, I.A., 1965. Handbook of Mathematical Functions. Dover, New York.

Carslaw, H.S., Jaeger, J.C., 1959. Conduction of Heat in Solids. Clarendon, Oxford, 510 pp.

Crank, J., 1975. The Mathematics of Diffusion. Clarendon, Oxford.

Crank, J., Nicolson, P., 1947. A practical method for numerical evaluation of solutions of partial differential equations of the heat-conduction type. Proc. Cambridge Philos. Soc. 43, 50–67.

Dodson, M.H., 1973. Closure temperature in cooling geochronological and petrological systems. Contrib. Mineral. Petrol. 40, 259–274.

Dunai, T.J., 2000. Helium diffusion in apatite revisited: is the previously inferred change in high temperature diffusion mechanism an artifact or a reality? In: Noble, W.P., O'Sullivan, P.B., Brown, R.W. (Eds.), 9th International Conference on Fission Track Dating and Thermochronology. Geological Society of Australia Abstracts Geol. Soc. Australia, Lorne, pp. 73–74.

Farley, K.A., 2000. Helium diffusion from apatite: general behaviour as illustrated by Durango fluorapatite. J. Geophys. Res. 105 (B2), 2903–2914.

Farley, K.A., Wolf, R.A., Silver, L.T., 1996. The effects of long alpha-stopping distances on (U–Th)/He ages. Geochim. Cosmochim. Acta 60, 4223–4229.

Fechtig, H., Kalbitzer, S., 1966. The diffusion of argon in potassium-bearing solids. In: Schaefer, O.A., Zahringer, J. (Eds.), Potassium–Argon Dating. Springer, Heidelberg, pp. 68–107.

House, M.A., Wernicke, B.P., Farley, K.A., Dumitru, T.A., 1997. Cenozoic thermal evolution of the central Sierra Nevada, California, from (U–Th)/He thermochronometry. Earth Planet. Sci. Lett. 151, 167–179.

House, M.A., Wernicke, B.P., Farley, K.A., 1998. Dating topography of the Sierra Nevada, California, using apatite (U–Th)/He ages. Nature 396, 66–69.

House, M.A., Farley, K.A., Kohn, B.P., 1999. An empirical test of helium diffusion in apatite: borehole data from the Otway basin, Australia. Earth Planet. Sci. Lett. 170, 463–474.

Lagerwall, T., Zimen, K.E., 1964. The kinetics of rare gas diffusion in solids. 772, EURATOM, Brussels.

Lippolt, H.J., Leitz, M., Wernicke, R.S., Hagedorn, B., 1994. (U+Th) Helium dating of apatite—experience from different geochemical environments. Chem. Geol. 112, 179–191.

Lovera, O.M., Richter, F.M., Harrison, T.M., 1989. The $^{40}Ar/^{39}Ar$ thermochronology for slowly cooled samples having a distribution of diffusion domain sizes. J. Geophys. Res. 94B, 17917–17935.

McDougall, I., Harrison, T.M., 1999. Geochronology and Thermochronology by the $^{40}Ar/^{39}Ar$ Method. Oxford Univ. Press, Oxford, 269 pp.

Meesters, A.G.C.A., Dunai, T.J., 2002. Solving the production–diffusion equation for finite diffusion domains of various shapes: Part II. Application to cases with α-ejection and non-homogenous distribution of the source. Chem. Geol., 186, 337–348 (this issue).

Reiners, P.W., Farley, K.A., 1999. Helium diffusion and (U–Th)/He thermochronometry of titanite. Geochim. Cosmochim. Acta 63, 3845–3859.

Reiners, P.W., Farley, K.A., 2001. Influence of crystal size on apatite (U–Th)/He thermochronology: an example from Bighorn Mountains, Wyoming. Earth Planet. Sci. Lett. 188, 413–420.

Reiners, P.W., et al., 2000. Helium and argon thermochronometry of the Gold Butte block, south Virgin Mountains, Nevada. Earth Planet. Sci. Lett. 178, 315–326.

Spotila, J.A., Farley, K.A., Sieh, K., 1998. Uplift and erosion of the San Bernardino Mountains associated with transpression along the San Andreas fault, California, as constrained by radiogenic helium thermochronometry. Tectonics 17, 360–378.

Wolf, R.A., Farley, K.A., Silver, L.T., 1996. Helium diffusion and low-temperature thermochronometry of apatite. Geochim. Cosmochim. Acta 60, 4231–4240.

Wolf, R.A., Farley, K.A., Kass, D.M., 1998. Modeling of the temperature sensitivity of the apatite (U–Th)/He thermochronometer. Chem. Geol. 148, 105–114.

Zeitler, P.K., Herczeg, A.L., McDougall, I., Honda, M., 1987. U–Th–He dating of apatite: a potential thermochronometer. Geochim. Cosmochim. Acta 51, 2865–2868.